ACS OMEGA

http://pubs.acs.org/journal/acsodf

Article

Swelling Characteristics and Interaction Mechanism of High-Rank Coal during CO_2 Injection: A Molecular Simulation Study

Kui Dong,* Zhiwei Zhai, and Bingyi Jia

Cite This: *ACS Omega* 2022, 7, 6911−6923

Read Online

ACCESS | Metrics & More | Article Recommendations | Supporting Information

ABSTRACT: In CO_2-enhanced coalbed methane (CO_2-ECBM) engineering, accurate knowledge of the interaction mechanism of CO_2 and coal matrix is crucial for improving the recovery of CH_4 and contributing to the geological sequestration of CO_2. This study is performed to prove the accuracy of molecular simulation and calculate the variation characteristics of pore structure, volumetric strain, mechanical properties, Fourier transform infrared (FT-IR) spectra, and the system free energy by molecular dynamics (MD) and grand canonical Monte Carlo (GCMC) methods. According to the obtained results, a relationship between pore structure, swelling strain, mechanical properties, chemical structure, and surface free energy was established. Then, the correlation of various coal change characteristics was analyzed to elucidate the interaction mechanism between CO_2 and coal. The results showed that (1) the molecular simulation method was able to estimate the swelling mechanism of CO_2 and coal. However, because the adsorption capacity of the molecular simulate is greater than that of the experiment and the raw coal is softer than the macromolecular structure, the molecular results are slightly better than the experimental results. (2) As pressure increased from 0 to 4 MPa, the intramolecular pores and sorption-induced strain changed significantly, whereas when the pressure increased from 4 to 8 MPa (especially at 6−8 Mpa), there was an increase of the intermolecular pores and mechanical properties and transition from elastic to plastic. In addition, when the pressure was >8 MPa, the coal matrix changed slightly. $ScCO_2$ with a higher adsorption capacity results in greater damage and causes larger alterations of coal mechanical properties. (3) The change of the coal matrix is essentially controlled by the surface free energy of the molecular system. $E_{valence}$ affects the aromatic structure and changes the volume of the intramolecular pores, thus affecting the sorption-induced strain change rate. E_{non} affects the length of side chains and the disorder degree of coal molecules and changes the volume of the intramolecular pores, thus affecting the mechanical property change rate. Our findings shed light on the dynamic process of coal swelling and provide a theoretical basis for CO_2 enhancing the recovery of CH_4 gas in coal.

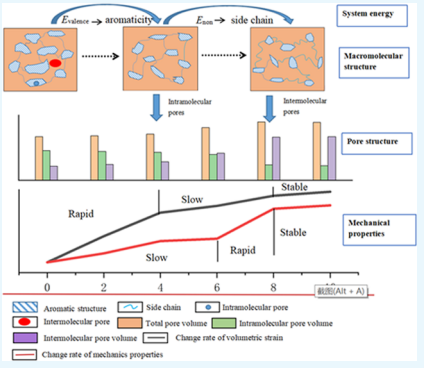

1. INTRODUCTION

CO_2-enhanced coalbed methane (CO_2-ECBM) recovery has a significant impact on CO_2 sequestration and unconventional gas extraction,[1−3] which will contribute to long-term safety production and alleviation of global warming.[4,5] CO_2 injected into the deep coal reservoir is converted into a supercritical state ($ScCO_2$),[6,7] which has a complex physical or chemical reaction with the coal seam, leading to coal structure rearrangement, coal matrix deformation, and changed mechanical properties of coal seams.[8−12] The physical properties of coal reservoir, such as porosity and permeability, are also changed,[13,14] thereby triggering numerous unexpected responses in coal seams upon CO_2 injection. Therefore, a proper understanding of the change mechanism of the coal matrix upon CO_2 injection is essential for optimization of the CO_2-ECBM techniques.

A number of investigations have explored the effect of CO_2 adsorption on coal pore structure. Kang et al.[15] found that the micropore volume decreases after supercritical CO_2 extraction. Liu et al.[16] found that, after the $ScCO_2$ treatment, the volume of the micropores with width <0.46 nm in high-volatile bituminous coal increased slightly, but the decrease in the volume of micropores with width <0.46 nm in the low-volatile bituminous, semianthracite, and anthracite coal became more pronounced. Zhang et al.[17] found that the volume of mesopores and macropores increases in high-, medium-, and low-rank coals. Liu et al.[18] found that after CO_2 treatment, the mesopore volume increased and the macropore volume decreased with the increase of coal rank. In other words, after the CO_2 treatment, the pore structure is changed, but it is not clear how the micropores, mesopores, and macropores change in different rank coals.

Researchers have developed relationships between coal mechanical property and coal rank. Ranjith et al.[19] compared the effect of lignite and bituminous coal and found that the

Received: November 21, 2021
Accepted: February 3, 2022
Published: February 15, 2022

strength reduction in bituminous coal is about 4.5 times higher than the strength reduction in lignite, and the best fitting curves for unconfined compressive stress (UCS) reduction with CO_2 saturation pressure exhibit different slopes for bituminous (15.3) and lignite coal (3.2), revealing that increasing CO_2 saturation pressure significantly affects the strength of bituminous coal. Similarly, Perera et al.[20] saturated bituminous coal at 8 MPa and 33 °C for 7 days and found that UCS decreased by 77.70%, which is significantly higher than UCS found by Ranathunga et al.[21] for low-rank coal saturated with CO_2 under 8 MPa and at 35 °C for 25 days. That is to say, CO_2−coal interaction leads to a more significant alteration in the mechanical properties of high-rank coal.

The inconsistency of changes in coal pore structure and mechanical properties is due to the diverse chemical structure of coal ranks. Low- and middle-rank coals contain many branches, while high-rank coals contain fewer branches and more aromatic rings. High-rank coals have more adsorption sites for CO_2 than low-rank coals and consequently more swelling potential upon CO_2 adsorption.[22,23] According to Griffith et al.[24] and Larsen et al.,[25] the adsorption of CO_2 with higher chemical potential reduces the surface energy of coal, which leads to the rearrangement of the macromolecules in coal to a more noncovalently associated structure. Therefore, the complex change process of the pore structure and mechanical properties is affected by the surface free energy of coal. To understand the different mechanisms coupled with each other, some scholars have used graphite and coal structure models to reveal specific processes of coal swelling caused by gas injection through molecular dynamics.[26−28] Zhang et al.[26] simulated the mechanical properties of methane bearing high-rank coal and found that with the increase of CH_4 content, the total surface free energy decreases, which leads to the reduction of the strength. Wang et al.[27] simulated a macromolecular rearrangement caused by CO_2 injection through molecular dynamics processes and found that the compression of closed pores and expansion of open pores together causes swelling of macromolecular volumes. Zhang et al.[28] used grand canonical Monte Carlo (GCMC) simulation to study the adsorption-induced deformation strain based on the deformation of organic carbon slit pore models and found that the molecules close to pore walls are parallel (tending to swell the pore) and play a dominant role in the deformation, and when the temperature increases, both swelling and shrinkage decrease due to a decrease in the adsorption density. However, coal is a complex compound with various functional groups and cross-linked bonds, and graphite and organic carbon slit pore models do not represent the structure of coal. Therefore, the simulation results are inconsistent. Wang et al.[27] showed that closed pores (diameter < 0.55 nm) decreased and the open pores (0.8 nm < diameter < 1.0 nm) increased. Zhang et al.[28] indicated that the pore aperture <0.55 nm shows no deformation and the pore aperture between 0.55 and 0.6 nm has the greatest swelling.

In this study, the high-rank coal Chengzhuang (CZ) from Qinshui Basin of China was selected as a research subject. The study mainly explores the influence of surface energy on pore structure, mechanical properties, and macromolecular structure after CO_2 treatment. First, the results of the experimental method and the molecular simulation method were compared to see whether they were consistent. If they were consistent, the reliability of the molecular simulation method was determined. Second, the molecular simulation method was used to study the change in coal deformation, mechanical properties, molecular structure, and surface free energy. Lastly, the relationship of various deformation characteristics was analyzed to illustrate the CO_2 swelling mechanism of high-rank coal. All molecular simulation calculations are performed in Materials Studio 2018 software.

2. SIMULATION AND CALCULATION METHODS

2.1. CZ Coal Molecular Structure. The macromolecular structure model of CZ (Figure 1) coal was constructed based on

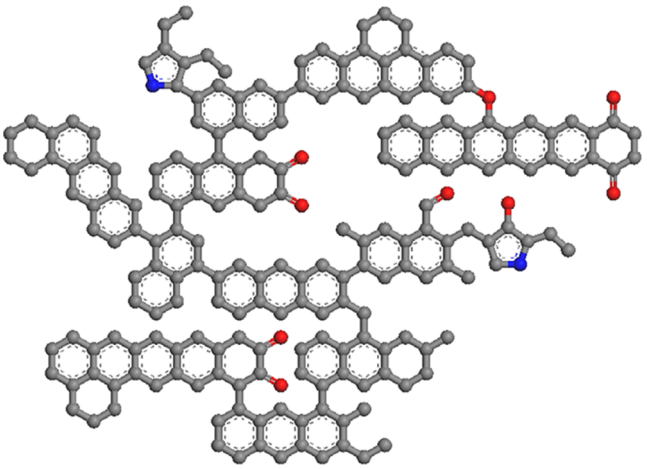

Figure 1. Model macromolecular structure in CZ coal.

the results of proximate and ultimate analyses, ^{13}C NMR spectrum, and XPS spectrum. The proximate and ultimate analyses of the model and the experiment are shown in Table S1, the ^{13}C NMR spectra of the model and the experiment are shown in Figure S1. On the whole, the model parameters agreed well with the experimental parameters, except for lower chemical shifts and a smaller area of the oxygen carbon zones in the CZ model compared with those in the experimental data.[29]

2.2. CO_2 Injection Simulation Process. *2.2.1. Simulation Model Construction.* First, a supercell containing 100 CZ coal molecules was constructed, and the structure of the supercell model was optimized.[30] The geometry optimization task in the Forcite module was used to optimize the structure of the model. The final configuration was an optimized coal model with the lowest energy. On the basis of the change in energy, Metropolis operation rules were applied to accept or reject the change for forming a new configuration. A periodic boundary condition was used in three dimensions, and the cell parameters were as follows: 6.77 nm × 6.77 nm × 6.77 nm (Figure 2). The Nose thermostat and NVT ensemble with a 1 fs time step were performed. For full interaction, 500 ps simulations were conducted. The Ewald method with a precision of 0.001 kcal/mol was used for electrostatic interactions, while van der Waals interaction was calculated using the atom-based option with a cutoff of 12.5 Å.

2.2.2. CO_2 Injection Process. CO_2 was simulated at 0, 2, 4, 6, 8, 10, 12, 14, and 16 MPa CO_2 injection pressure. The amount of CO_2 adsorbed at a fixed pressure is obtained by the fix pressure task in the Sorption module, and the COMPASS II force field,[31] a temperature of 298 K, and Metropolis operation rules[32] were used for the simulation.

To simulate the CO_2 injection process in the coal, the Adsorption Locator module from Materials Studio 2018 was used to place some CO_2 molecules in the box, according to the

https://doi.org/10.1021/acsomega.1c06566
ACS Omega 2022, 7, 6911−6923

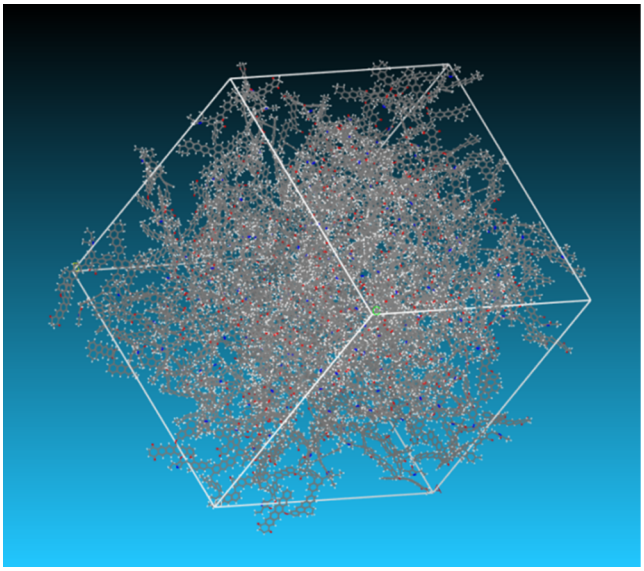

Figure 2. Supercell containing 100 CZ macromolecules.

average adsorption in different fixed-pressure adsorptions. Then, the optimization of macromolecular structures, containing CO_2, was carried out using the isothermal isobaric ensemble (NPT) and selecting the Andersen temperature-control method (298 K) and the Berendsen pressure control method. The duration of the simulation was 300 ps, the step size was 1 fs, and the sampling interval was 100 fs. The last 50 ps of data were collected for analysis.[27]

2.2.3. Isothermal Adsorption of CO_2. The isothermal adsorption calculations were conducted by the adsorption isotherm task in the Sorption module. The force field used was COMPASS II. The convergence criterion for energy was 5×10^{-4} kcal/mol, and the fugacity step was 20. The maximum number of iterations and equilibration steps were set as 50 000 and 10 000, respectively. The Ewald sum method was used for electrostatic action, and van der Waals force was calculated via the atom-based method with cubic spline truncation. The cutoff distances for both electrostatic action and van der Waals force were set as 12.5 Å. To ensure balance in the system, 2×10^7 GCMC steps were adopted.

2.2.4. Mechanical Property Simulation. The mechanical properties were simulated by the mechanical properties task in the Forcite module. The method is constant, the number of steps for each strain is 11, and the maximum strain amplitude is 0.1.

Young's modulus, Poisson's ratio, and stress−strain curves are usually used to characterize the mechanical properties.

(1) Unconfined compressive stress (UCS)[33]

$$\mathrm{UCS} = P/A \tag{1}$$

where P is the maximum load at failure of the specimen, N, and A is the sample area, mm^2.

(2) Young's modulus[34]

$$E = \mu\frac{3\lambda + 2\mu}{\lambda + \mu} \tag{2}$$

(3) Poisson's ratio[34]

$$\nu = \frac{1}{2}\frac{\lambda}{\lambda + \mu} \tag{3}$$

where E is Young's modulus, GPa; ν is Poisson's ratio; and λ and μ are Lamé coefficients, GPa.

(4) Stress−strain curves.

For each configuration, several strains are applied, resulting in a strained structure. The resulting structure is then optimized, keeping the cell parameters (and hence the strain) fixed to allow for internal relaxation. The number of steps for each strain is 11, the maximum strain amplitude is 0.003, and strain patterns are 100000 and 010000.

This defines a range of values, {−0.003, −0.001, 0.001, 0.003}, applied to each strain pattern[35,36]

strain pattern 100000 gives$e$

$$= \{-0.003, 0, 0, 0, 0, 0\},\ \{-0.001, 0, 0, 0, 0, 0\},\ \{0.001, 0, 0, 0, 0, 0\},\ \{0.003,\ 0, 0, 0, 0, 0\}$$

strain pattern 010000 gives e

$$= \{0, -0.003, 0, 0, 0, 0\},\ \{0, -0.001, 0, 0, 0, 0\},\ \{0,\ 0.001, 0, 0, 0, 0\},\ \{0, 0.003, 0, 0, 0, 0\}$$

These are then used to generate the metric tensor: G, GPa.

Each strain pattern represents the strain matrix in Voigt notation. It is converted to the strain matrix, ε, such that $\varepsilon(0,0) = e(0)$, $\varepsilon(1,1) = e(1)$, $\varepsilon(2,2) = e(2)$, $\varepsilon(2,1) = \varepsilon(1,2) = 0.5*e(3)$,...

$$G = H_0{}'\,(2\varepsilon + I)H^0 \tag{4}$$

where H_0 is formed from the lattice vectors, I is the identity matrix, and $H_0{}'$ is the transpose of H_0.

From G, the new lattice parameters can be derived; these parameters are used to transform the cell parameters (fractional coordinates are held fixed).

2.3. Volumetric Strain Deformation Models. The total volumetric strain, including sorption-induced strain variation and mechanical strain variation, is as follows

$$\varepsilon = \varepsilon^a + \varepsilon^m \tag{5}$$

where ε, ε^a, and ε^m are the total volumetric, sorption-induced, and mechanical strain, respectively.

The mechanical strain caused by stress can be written as[37,38]

$$\varepsilon^m = -\frac{P}{E_s}(1 - 2\nu_s) \tag{6}$$

where E_s and ν_s are Young's modulus and Poisson's ratio of the coal matrix, respectively, and P is gas pressure, MPa.

The linear strain was derived as[39]

$$\varepsilon = -\frac{\gamma A \rho_s}{E_s} f(x, \nu_s) \tag{7}$$

where

$$f(x, \nu_s) = \frac{[2(1-\nu_s) - (1 + \nu_s)cx][3-5\nu_s - 4(1 - 2\nu_s)cx]}{(3 - 5\nu_s)(2 - 3cx)} \tag{8}$$

and where $c = 8\sqrt{2/3\pi} = 1.2$.

From this structure model, porosity can be calculated as

$$\phi = 1 - 3\pi x^2(1 - cx) \tag{9}$$

Since the high-pressure gas compresses the coal solid, the strain caused by this pressure alone is[40]

https://doi.org/10.1021/acsomega.1c06566
ACS Omega 2022, 7, 6911−6923

$$\varepsilon = -\frac{P}{E_s}(1 - 2\nu_s) \tag{10}$$

Combining adsorption and pressure compression strains and using $\gamma = \Phi/A$, the overall strain can be derived as

$$\varepsilon = -\frac{\phi\rho_s}{E_s}f(x, \nu_s) - \frac{P}{E_s}(1 - 2\nu_s) \tag{11}$$

With a Langmuir adsorption isotherm model

$$n^a = \frac{abP}{1 + aP}\varepsilon = -\frac{P}{E_s}(1 - 2\nu_s) \tag{12}$$

and assuming the fugacity is equal to pressure for calculation simplicity, the surface potential can be calculated as

$$\phi = \int_0^P V^a \, dP - RT\int_0^P \left(\sum_{i=1}^{C} n_i^a d \ln f_i\right) = \int_0^P V^a \, dP - RT\int_0^P \frac{ab}{1 + aP} \, dP = \int_0^P V^a \, dP - RTb \ln(1 + aP) \tag{13}$$

V_a is the volume change for unit mass of adsorbent, cm^3/g. Its relationship with strain is

$$V^a = \frac{\varepsilon_V}{\rho} = \frac{\varepsilon_V}{\rho_s(1 - \phi)} = \frac{3\varepsilon}{\rho_s(1 - \phi)} \tag{14}$$

The volumetric strain can be obtained from eqs 13 and 14 being substituted into eq 15

$$\varepsilon = -\frac{\phi\rho_s}{E_s}f(x, \nu_s) - \frac{P}{E_s}(1 - 2\nu_s) \tag{15}$$

where ρ_s is the solid density, cm^3/g. E_s and ν_s are Young's modulus and Poisson's ratio of the coal matrix, respectively.

When the simple fitting method is adopted to describe the volumetric deformation variations, the model can be simplified as[41]

$$\varepsilon = -\frac{m\rho_s}{E_s} - \frac{P}{E_s}(1 - 2\nu_s) \tag{16}$$

where m is a fitting parameter determined by coal characteristics.

2.4. Surface Potential. The strain variations are linked with surface potential. The surface potential for compressible solid adsorbent can be written as[42]

$$\Phi = \int_0^P V^a \, dP - RT\int_0^P \left(\sum_{i=1}^{C} n_i^a \, d \, Ln \, P\right) \tag{17}$$

where Φ is the surface potential, Kcal/mol; V^a is the solid volume change at the equilibrium adsorption pressure, cm^3/g; P is the gas pressure, MPa; n_i^a is the amount of adsorbed gas, N; R is the gas constant, 8.314J/(mol·K); and T is the temperature, K.

3. RESULTS AND DISCUSSION

3.1. Experiment and Molecular Simulation Comparison. The variation characteristics of the CO_2-adsorption capacity and mechanical properties obtained by the experiment and molecular simulation have been compared. The experimental results of the CZ coal matrix swelling characteristics under different CO_2 injection pressures were studied by Wang et al.[43]

3.1.1. CO_2 Adsorption Capacity. Figure 3 shows the results of the CO_2 absolute adsorption capacity obtained by the experiment and simulation, respectively. The absolute adsorption capacity obtained by both methods increased with the increasing CO_2 injection pressure, and the CO_2 adsorption capacity increased fastest when the injection pressure was lower than 4 MPa but increased slowly when the pressure was greater than 4 MPa. Although the adsorption curves obtained by the experiment and simulation are analogous, the amount of CO_2 adsorption obtained by simulation is greater than that obtained by the experiment. This is because samples used by Wang et al.[43] were core coals, and the volume of pores in the experiment was smaller than that of the molecular simulation, resulting in an underestimation of CO_2 adsorption capacity in the volumetric methane adsorption experiment.[44]

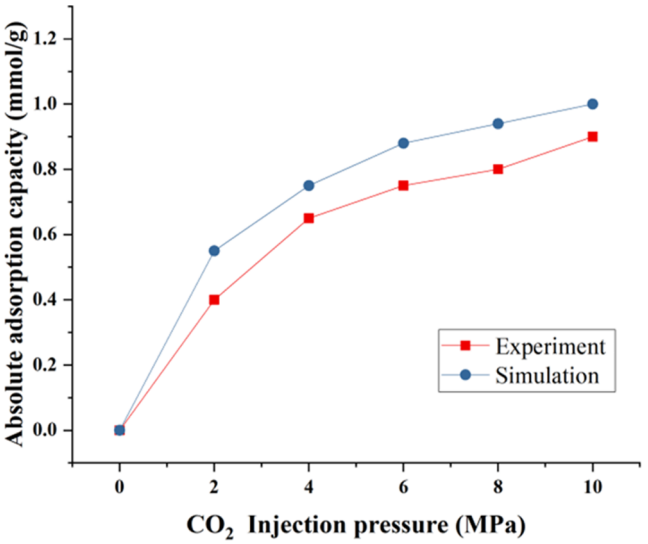

Figure 3. Relationship between the absolute adsorption capacity of CZ coal and CO_2 injection pressure.

3.1.2. Volumetric Swelling Strain. Figure 4 shows the relationship between volumetric swelling strain and CO_2 injection pressure from the experiment and simulation. Because

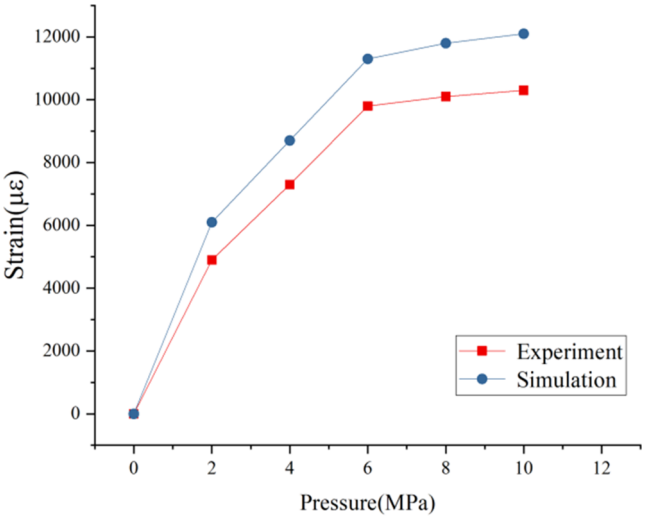

Figure 4. Relationship between volumetric swelling strain and CO_2 injection pressure obtained from the experiment and simulation.

https://doi.org/10.1021/acsomega.1c06566
ACS Omega 2022, 7, 6911−6923

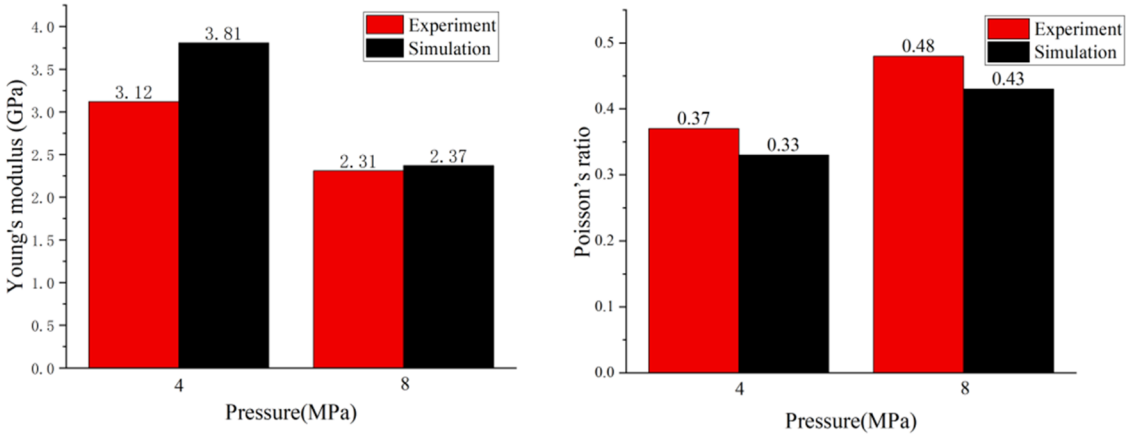

Figure 5. Distinction of Young's modulus and Poisson's ratio between the experiment and simulation.

the CO_2 adsorption capacity calculated using molecular simulation is stronger than that of the experiment, the simulated volumetric swelling strain is larger than the experimental one.

3.1.3. Mechanical Properties. Figure 5 shows the distinction of Young's modulus and Poisson's ratio between the experiment and simulation at 4 and 8 MPa. The Young's modulus values obtained by the experiment are larger than those obtained by the simulation, while the Poisson's ratio values obtained by the experiment are smaller than those obtained by the simulation. The higher the Young's modulus value, the smaller the elastic modulus deformation of the material, and the easier it is for the material to deform. This indicates that the raw coal sample is softer than the coal macromolecular structure. Both results show that in the subcritical CO_2 injection stage, Young's modulus decreased while Poisson's ratio increased slowly. During the transition phase of CO_2 injection pressure, the change values of Young's modulus and Poisson's ratio increased. This shows that the phase transition softened the coal matrix, and with the increase of CO_2 injection pressure, the deformation of coal and rock changed from brittleness to plasticity.

The results of the molecular simulation are better than those of the experiment because the molecular simulation is in an ideal environment; however, their changing trends are consistent. Therefore, molecular simulation is an effective method to study the coal matrix alterations during CO_2 injection into coal. In addition, it can study the interaction mechanism of CO_2−coal.

3.2. Coal Matrix Deformation. *3.2.1. Pore Structure Deformation.* Table 1 shows the pore structure parameters of coal under different CO_2 injection pressures. The pore size distribution was calculated using Poreblazer software.[45] When the injection pressure increased, the total pore volume, porosity, and intermolecular pore (>0.4 nm) volume increased, whereas the intramolecular pores (<0.4 nm) decreased. When the pressure was less than 4 MPa, the volume of intramolecular pores changed rapidly while the volume of intermolecular pores changed slowly. At 4−8 MPa, the pore structure parameters changed and the proportion of intermolecular pores exceeded that of the intramolecular pores; the porosity changed from 5.25 to 6.61%. After 8 MPa, the pore volume remained stable and the porosity decreased from 6.61 to 6.49%.

Table 1. Coal Macromolecular Pore Structure Parameters under Different CO_2 Injection Pressures

gas pressure (MPa)	coal volume (nm^3)	total pore volume (cm^3/g)	intramolecular pore volume (cm^3/g)	intermolecular pore volume (cm^3/g)	porosity (%)
0	34.66	0.0501	0.0340	0.0161	5.12
2	35.31	0.0513	0.0332	0.0181	5.23
4	35.51	0.0530	0.0219	0.0211	5.25
6	35.51	0.0605	0.0194	0.0311	6.05
8	36.01	0.0672	0.0177	0.0495	6.61
10	35.80	0.0668	0.0166	0.0502	6.62
12	35.48	0.0666	0.0162	0.0504	6.63
14	35.49	0.0666	0.0161	0.0505	6.63
16	35.44	0.0664	0.0160	0.0504	6.63

The pore size distribution (PSD) of CZ coal determined from CO_2 adsorption is shown in Figure 6. (When the pressure is >12 MPa, the curves of PSD do not change obviously, which is not shown in Figure 6.) The pores are mainly distributed in the pore size range of 0.3−0.9 nm, and the pore volume presents a multipeak distribution (generally two to three). There are two main peaks at 0.35−0.40 (intramolecular pore) and 0.65−0.75 nm (intermolecular pore). After CO_2 treatment, both the peak positions and peak shapes are significantly altered. At 0, 4, 8, and 12 MPa, the peak values of intramolecular pore are 0.075, 0.080, 0.088, and 0.089 $cm^3/g/nm$ and the peak values of intermolecular pore are 0.0063, 0.053, 0.076, and 0.065 $cm^3/g/nm$, respectively. The two peak values are higher in CZ coal after treatment, the width of the intramolecular pore peak is reduced, and the intermolecular pores are increased. This finding illustrates that after CO_2 adsorption, the intramolecular pores were compressed, providing space for the formation of intermolecular pores, and $ScCO_2$ treatment has a remarkable influence on the micropore distribution of high-rank coal. Chen et al.[46] studied the influence of $ScCO_2$ on the pore structure of low- and high-rank coal and concluded that the largest increase in macropore volume is observed in low-rank coal and the greatest reduction of micropore volume in high-rank coal. This phenomenon can also be found in the studies of Gao et al.,[47] Cheng et al.,[48] Juan et al.,[49] and Liu et al.[50]

To compare the PSD results with conventional pore measuring technology, LP-N_2-Ad were carried out using an automated gas sorption analyzer (Autosorb iQ-MP, Quantachrome Instruments, Germany), in accordance with the national standards (GB/T 21650.2-2008, 2008;[51] GB/T 21650.3-2011, 2011[52]), and the calculation results were obtained by DA and NLDFT models. Figure 7 shows the PSD curves of simulation and DA and NLDFT models. The PSD curves of simulation and NLDFT are similar are significantly different from the DA model

https://doi.org/10.1021/acsomega.1c06566
ACS Omega 2022, 7, 6911−6923

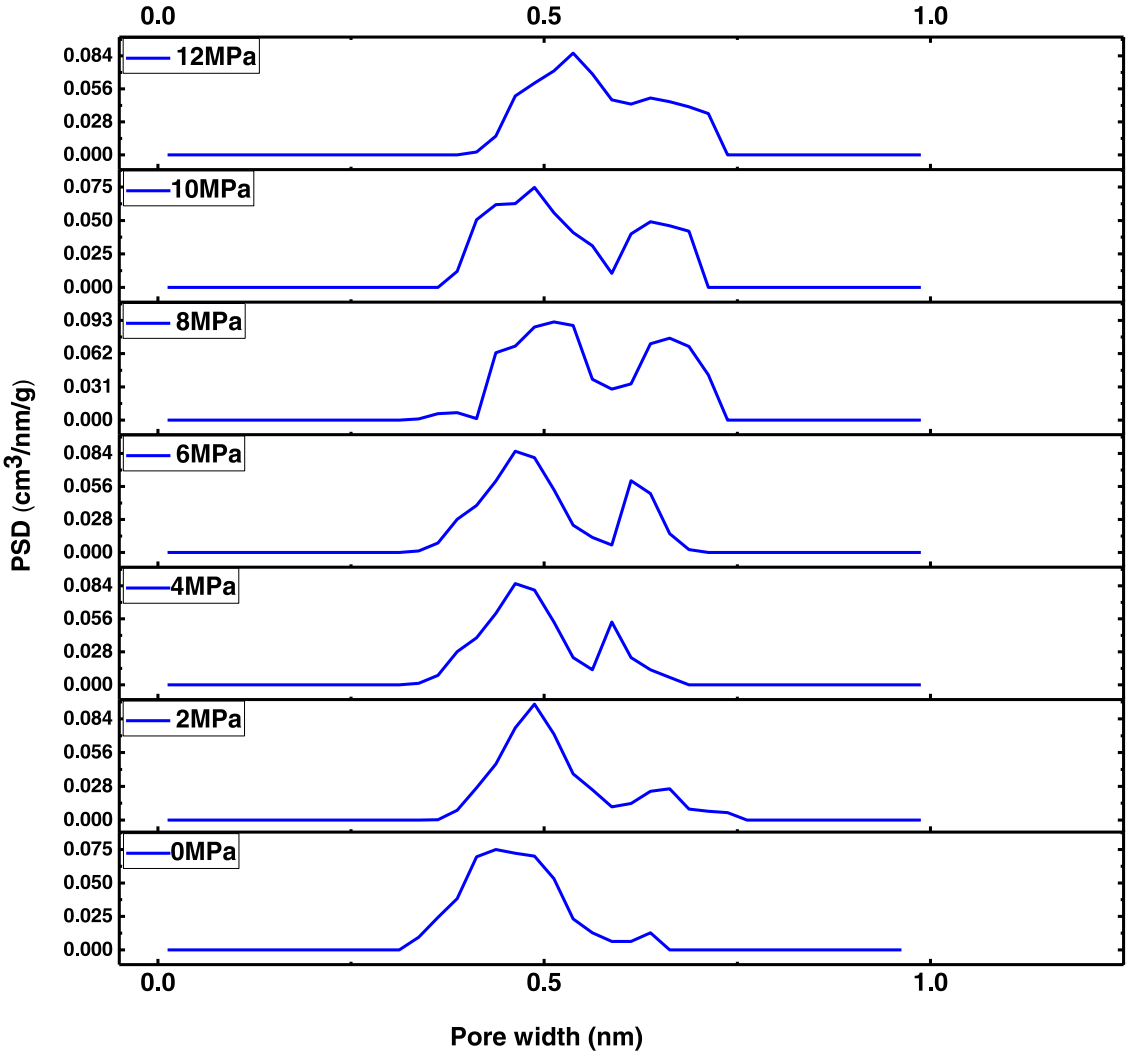

Figure 6. Pore size distribution of CZ coal at different CO_2 injection pressures.

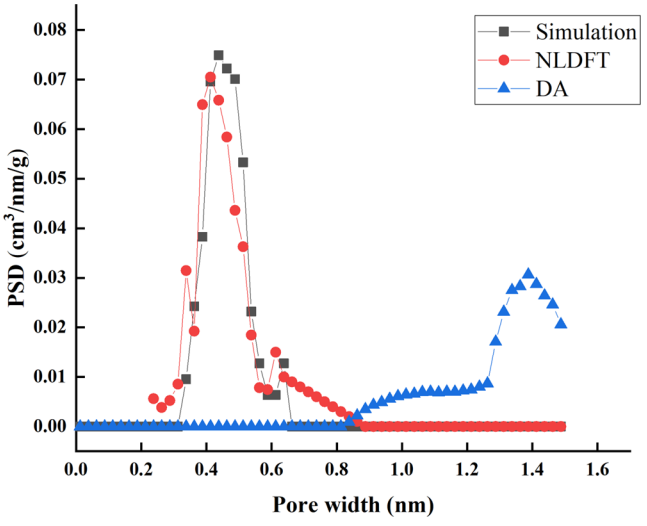

Figure 7. Comparison and analysis of PSD by simulation and NLDFT and DA models.

result. The DA model does not consider changes of these parameters or the influence of pore shape on gas molecule accumulation; therefore, the calculation results of this model may deviate further.[53] The analysis results of simulation and the NLDFT model, which describe the adsorption behavior in the narrow space of micropores, are more accurate. The pore volume obtained by the NLDFT model is slightly lower than the analysis result of the simulation, which might be caused by the effect of ash in the coal matrix.[54] This indicates that the molecular simulation method is accurate for analyzing the pore size distribution of micropores in coal.

3.2.2. Volumetric Strain Deformation. The relationship between swelling strains and CO_2 injection pressure is shown in Figure 8. The volumetric strain deformation caused by CO_2 adsorption is mainly composed of two parts: the sorption-induced strain caused by CO_2 adsorption and the mechanical strain caused by effective stress change. According to Section 2.2, the sorption-induced strain can be obtained by subtracting the mechanical strain from the volumetric strain. The volumetric strain and sorption-induced strain change values at pressure <4 MPa are 1.5 times those at 4−8 MPa. But the mechanical strain is different from them. The mechanical strain curve increased slowly at 0−6 MPa and increased rapidly at 6−8 MPa. When the pressure was >8 MPa, the deformation change in all of them was not obvious. It could be seen that the sorption-induced swelling is a dominant factor in volumetric strain. Zhao et al.[41] also obtained the same result from experimental research.

https://doi.org/10.1021/acsomega.1c06566
ACS Omega 2022, 7, 6911−6923

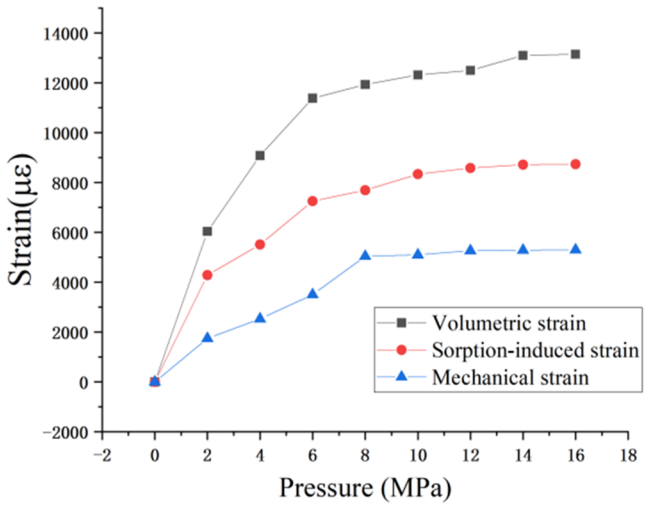

Figure 8. Relationship between swelling strain and different CO_2 injection pressures.

3.2.3. Effects of Pore Structure on Swelling Strain. As shown in Table 1 and Figures 3 and 9, when pressure ranged within 0−4 MPa, we found that the absolute adsorption capacity increased from 0 to 0.8 mmol/g, the volumetric and sorption-induced swelling strain increased from 0 to 9000 and 0 to 4800, respectively, and the intramolecular pore reduced from 0.0340 to 0.0219. When pressure ranged within 4−8 MPa, the absolute adsorption capacity increased from 0.8 to 1.0 mmol/g, the volumetric and sorption-induced swelling strain increased from 0 to 12 000 and 0 to 5500, respectively, and the intramolecular pore reduced from 0.0219 to 0.0177. However, when pressure was at the >8 MPa stage, the absolute adsorption capacity, intramolecular pore, and swelling strain are not obviously changed.

This phenomenon can be attributed to the CO_2 adsorption characteristics of coal. The swelling of the coal matrix is related to the amount of CO_2 adsorbed. The higher amount of CO_2 adsorbed, the greater the increase in volumetric and sorption-induced swelling strain, and the pore structure affects the adsorption of CO_2, thereby affecting the volumetric and sorption-induced swelling strain of coal. The swelling caused by the adsorption of CO_2 changes the pore structure of coal, and this change of the pore structure of coal also affects the adsorption capacity of CO_2. In the initial stage of adsorption, the coal matrix contains <0.4 nm pores, and there is no gas adsorbed in the coal matrix; CO_2 tends to be adsorbed in pores <0.4 nm. Therefore, CO_2 can be quickly adsorbed in the pore structure of coal in the low-pressure stage, and this causes volumetric and sorption-induced swelling strain to increase rapidly at 0−4 MPa. With the increase of the amount of CO_2 adsorbed, the macromolecular structure of coal changes significantly, resulting in a decrease in the pore content of <0.4 nm with increasing pressure. Therefore, the rate of coal adsorption of CO_2 slows down with the increase of pressure. Thus, when the adsorption amount of CO_2 increases rapidly, the swelling stress changes significantly (0−4 MPa), then changes slowly when the <0.4 nm pore content decreases and the increase in CO_2 adsorption decreases (4−6 MPa) and finally becomes stable.

The mechanical strain changes correlate with intermolecular pores and are discussed in the next section.

3.3. Coal Mechanical Properties. The following sections discuss the various mechanical properties of coal: unconfined compressive stress (UCS); Young's modulus (E); Poisson's ratio (ν); and stress−strain features for three stages, subcritical stage (<6 MPa), transfer stage (6−8 MPa), and supercritical stage (>8 MPa).

3.3.1. UCS, Young's Modulus, and Poisson's Ratio. The modified characteristics of UCS are shown in Figure S2 and Table 2. With an increase in the CO_2 saturation pressure, UCS of the coal decreased. At pressures from 0 to 6 MPa, UCS reduced slowly. When CO_2 injection pressure increased from 6 to 8 MPa, CO_2 transformed from a sub- to a supercritical state. The UCS reduction amplitude in coal was subjected to a sudden increase from 30.76 to 52.75%. However, when the pressure was >8 MPa, especially when the pressure was >12 MPa, there was no change in UCS with increasing pressure. According to Zeng et al.,[54] when pressure increased, the contribution to the fracture (cleat) aperture change increased from zero to a peak value and then dropped to zero, reducing the diffusion capacity of CO_2 with increasing pressure. Thus, UCS changed less at higher supercritical CO_2 pressures.

The coal matrix swelling caused by CO_2 adsorption affected Young's modulus and Poisson's ratio (Figures S3 and S4 and

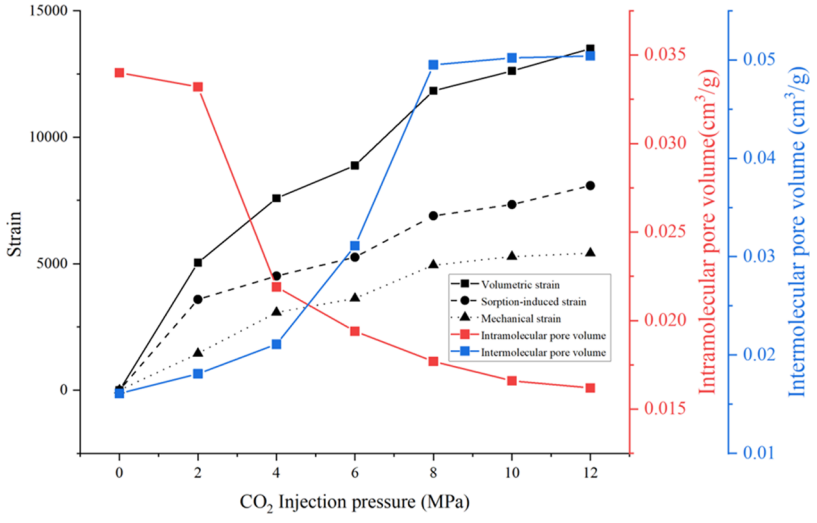

Figure 9. Relationship of pore structure and swelling strain.

https://doi.org/10.1021/acsomega.1c06566
ACS Omega 2022, 7, 6911−6923

Table 2. Mechanical Parameter Changes of CZ Coal with Different CO_2 Injection Pressures

pressure (MPa)	UCS (MPa)	ΔUCS (%)	E (GPa)	ΔE (%)	ν	Δν (%)
0	68.71		6.46		0.26	0
2	57.57	16.20	5.34	17.33	0.3	15.38
4	52.74	23.23	3.81	41.02	0.33	26.92
6	47.57	30.76	3.51	45.66	0.36	38.46
8	32.46	52.75	2.37	63.31	0.43	65.38
10	31.89	53.57	2.06	68.11	0.44	69.23
12	31.31	54.44	1.95	69.81	0.45	73.07
14	31.20	54.59	1.93	70.12	0.45	73.07
16	31.22	54.59	1.91	70.43	0.45	73.07

Table 2). Similar to UCS, these variations could be divided into three stages. At the subcritical CO_2 saturation stage (<6 MPa), Young's modulus decreased by 45.56% and Poisson's ratio increased by 38.46%. In the transfer stage (6 MPa < pressure < 8 MPa), compared with the subcritical CO_2-saturation stage, Young's modulus was reduced by 1.5 times while Poisson's ratio was increased by 1.5 times (Young's modulus: 63.31%; Poisson's ratio: 65.38%). When CO_2-saturation pressure increased beyond 8 MPa, Young's modulus and Poisson's ratio did not cause a perceptible change.

The change in mechanical properties shown in the three stages is related to the brittle−ductile properties and the polymeric structure of coal. When CO_2 was absorbed into the coal matrix, swelling changed its cross-linking and polymeric structure.[45] This improved the ductile properties of coal, reduced Young's modulus, and increased Poisson's ratio. Supercritical CO_2 has a higher plasticizing effect than subcritical CO_2, and the decrease in Young's modulus and the increase in Poisson's ratio become larger. When the saturation pressure of CO_2 was further increased, the fracture (cleat) aperture of coal could be closed, and the diffusion capacity of CO_2 was reduced. Thus, the plasticization capacity of coal was stable at high pressure (>8 MPa).

3.3.2. Stress−Strain Features. Figure 10 shows the stress−strain curves of the coal matrix. (The curves of 14 and 16 MPa are overlapped with 12 MPa, which are not shown in Figure 10.) Under the influence of CO_2 injection pressure, the stress−strain curves of CZ coal are different. The compression deformation was induced by stress. The stress−strain curves could be divided into four parts: compaction, elastic deformation, crack expansion, and peak strength stages.

(a) Compaction stage: with a gradual increase in axial pressure, the curve of this process is concave; the initial curve is relatively stable and then begins to rise, indicating that the slope of the curve increases and the stiffness of the coal rock increases. With the gradual increase in the axial stress, the pre-existing pores and cracks in the coal and rock were compressed or even closed. A small change in stress in this stage causes a large deformation. As the compressibility of the pores and cracks decreased, under the same stress, the amount of deformation gradually decreased, which caused concave stress−strain curves in the initial stage.

(b) Elastic deformation stage: In the previous stage, the coal sample was compacted, the degree of pores and fissures was reduced, and the density of coal became larger. In this stage, there is a linear relationship between the strain and stress of the coal, and the stress−strain curves can be regarded as a straight line.

(c) Crack expansion stage: with a further increase in the axial stress, coal enters the stage of crack expansion, and the stress−strain curves enter the stage of nonlinear change again. During this process, the slope of the stress−strain curves decreases, and the stiffness of the coal sample also begins to decrease. Due to the generation of cracks, the increase rate of the volumetric strain of the coal sample decreased.

(d) Peak strength stage: the coal and rock rupture, and the stress−strain curve drops as the crack continues to increase. Since the macromolecular structure of coal cannot simulate coal rupture, the curve declines.

The stress−strain curves are different at subcritical and supercritical CO_2 adsorption pressures. The elastic deformation in the supercritical CO_2 stage was greater than that in the subcritical CO_2 stage, indicating that the supercritical CO_2 adsorption reduced the elastic section of the stress−strain curve and enhanced the plasticity of the coal matrix.

3.3.3. Effect of Pore Structure on Mechanical Property. Previous studies have shown that mechanical properties are related to the coal pore structure. For example, Masoudian et al.[55] observed a decrease in the size of the particles and considered that such changes caused a reduction in strength. Li et al.[56] showed that the mechanical strength weakened in relation to an increase in macropores. However, it should be noted that experimental methods can only describe qualitatively rather than quantitatively.

As shown in Figure 11, the relationship between the pore structure and UCS is described quantitatively. The change in intermolecular volume is negatively correlated with the change in UCS. At 0−6 MPa, the intermolecular pores increased from

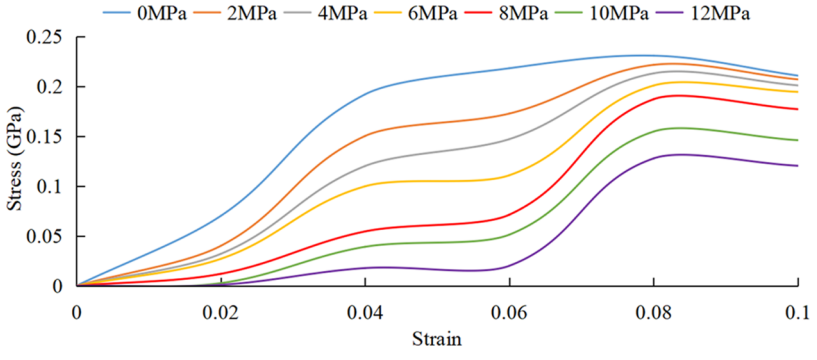

Figure 10. Stress−strain curves of CZ coal with different CO_2 injection pressures.

https://doi.org/10.1021/acsomega.1c06566
ACS Omega 2022, 7, 6911−6923

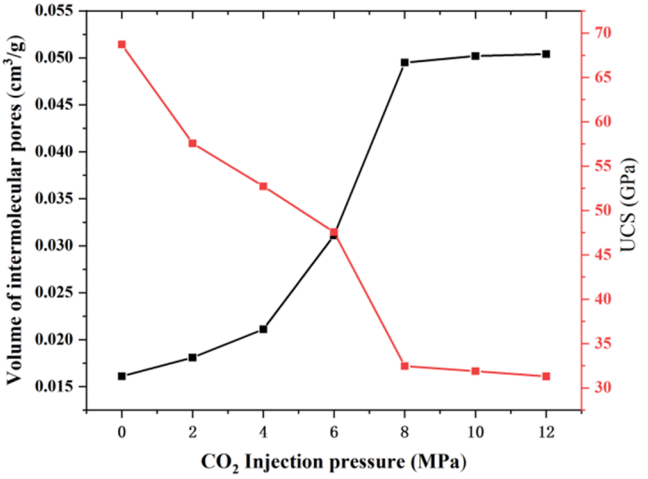

Figure 11. Relationship of pore structure and UCS.

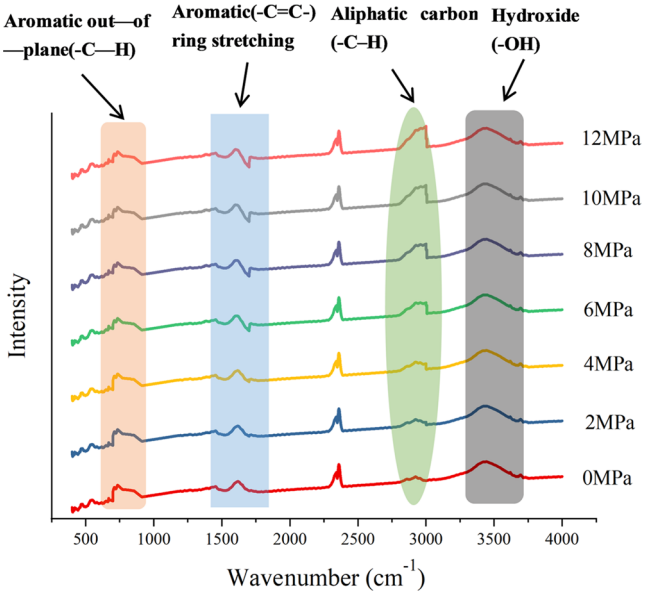

Figure 12. FT-IR spectra of CZ with different CO_2 injection pressures.

0.0161 to 0.0311 cm^3/g and UCS reduced to 30.76%. At 6−8 MPa, the intermolecular pores increased from 0.0311 to 0.0495 cm^3/g and UCS reduced to 52.75%. When the pressure was >8 MPa, the intermolecular pores and volume remained stable. The increased intermolecular pores indicated that the original pores were enlarged by swelling, the plasticity of the coal matrix increased, and the mechanical properties of coal weakened. The relationship between the pore structure, Young's modulus, and Poisson's ratio is shown in Figure S5, in which the correlation is similar to that with UCS. Supercritical CO_2 has higher diffusivity and lower viscosity[57] and adsorbs pores more easily than subcritical CO_2, and thus, the impact of supercritical CO_2 on coal is greater than that of subcritical CO_2.

3.4. Coal Macromolecular Structural Properties. The effect of CO_2 on coal macromolecules is mainly seen in two ways. (1) The difference in the macromolecules of low−middle- and high-rank coal. In the coalification process, the number of side chains and functional groups were constantly reduced due to the weak binding force of side chains and functional groups.[58] (2) The diversity of interactions between CO_2 and coal functional groups. The adsorption order of CO_2 is aromatic rings >−C2O> C═O > $-CH_3$ > −OH.[59]

FT-IR spectra can be obtained to derive molecular structure information by analysis of the position and intensity of absorption peaks of different functional groups.[60] The basic structural units in coal, such as alkyl side chains, oxygen-containing groups, or aromatic rings, can be analyzed in detail on the basis of changes in the absorption peak intensity. To determine changes in the characteristic absorption peaks in the infrared spectrum after $ScCO_2$ injection with different pressures, the FT-IR spectrogram is divided into four parts: (1) hydroxyl groups (−OH, 3700−3100 cm^{-1}), (2) aliphatic structures ($-CH_X$, 3000−2800 cm^{-1}), (3) aromatic structures (1600 cm^{-1}), and (4) aromatic out-of-plane structures (−C−H−, 900−700 cm^{-1}); the FT-IR spectra of the functional-group region are shown in Figure 12.

The intensity of the −OH group absorption peak for CZ coal had no obvious changes after CO_2 treatment (Figure 12, gray circle). As coal rank increases, the carbon content gradually increases and the oxygen content decreases. CZ, which is high-rank coal, has low oxygen content and high carbon content, and the coal matrix swelling caused by CO_2 adsorption did not change the oxygen content. As a result, the −OH group showed almost no changes with CO_2 treatment.

The 3000−2800 and 1600 cm^{-1} wavelengths changed more significantly under the supercritical CO_2 pressure than under the subcritical CO_2 pressure, resulting in a sudden enhancement of aliphatic side chains ($-CH_X$) and a reduction of aromatic carbon (−C═C−) (Figure 12, green and blue circles). −C═C− of aromatic structures, particularly polycyclic aromatic hydrocarbons (PAHs), have low bond dissociation energy and are easily broken. The longer the aliphatic side chains, the smaller the energy need for bond dissociation, and R_2-CH_2 breaks easier than $-CH_3$. CZ coal has high PAH content and low aliphatic content, and the length of the aliphatic side chains is relatively short. After CO_2 treatment, the aliphatic side chains in their original composition are expected to show almost no changes, as the PAHs are broken and changed into aliphatic side chains. As a result, the aromatic structures are obviously weakened and aliphatic side chains are increased.

The transmittance peak in the 900−700 cm^{-1} wavelength region indicates the vibration of aromatic out-of-plane C−H.[46,47] We observed that there was a slight increase. As explained by Lin et al.,[60] the coal samples under $ScCO_2$ treatment predominantly displayed substitution reactions, which led to the increase of substituents. As the coal rank increased, the bond dissociation reactions also increased. Because CZ is high-rank coal, the change of substituents is not strong. Therefore, the band change of 900−700 cm^{-1} is not obvious.

3.5. Coal System Energy Properties. The total energy (E_{total}) consists of valence ($E_{Valence}$) and nonvalence (E_{non}) ($E_{total} = E_{valence+}E_{non}$) energies. From Table 3, $E_{valence}$ and E_{non} decreased with different CO_2 injection pressures, indicating that the position of the atom in the macromolecular structure and the distance between the molecules are changed.

3.5.1. Variation of $E_{Valence}$ of Coal under Different CO_2 Injection Pressures. $E_{Valence}$ is the main form of the stable molecular structure. The change of valence energy causes atom displacement, and the displacement of atoms leads to bond stretching (E_B) and angle (E_A), torsion (E_T), and inversion (E_I) changes in the model structure. The greater the aromaticity of coal, the higher the $E_{Valence}$ of coal. From Table 3, $E_{valence}$ reduced from 23 451 to 23 333 Kcal/mol, which implies a decrease of aromaticity, causing the molecular structure to loosen.

https://doi.org/10.1021/acsomega.1c06566
ACS Omega 2022, 7, 6911−6923

Table 3. Energy Comparison of CZ Coal with Different CO_2 Injection Pressures (Kcal/mol)

		$E_{Valence}$				E_{non}	
gas pressure (MPa)	E_{Tot}	E_B	E_A	E_T	E_I	E_{vdW}	E_e
0	24197.37	1361.24	1342.14	20566.71	181.2	873.45	−127.37
2	24169.25	1360.11	1339.63	20565.18	167.89	863.84	−127.4
4	24116.86	1352.94	1325.11	20554.88	160.18	851.16	−127.41
6	24072.91	1345.98	1320.93	20552.71	157.84	829.23	−133.78
8	23994.15	1341.91	1315.02	20548.01	154.91	768.24	−133.94
10	23949.84	1321.61	1314.99	20547.87	152.74	753.19	−140.56
12	23916.2	1321.55	1314.27	20547.33	151.14	722.97	−141.06
14	23913.01	1321.38	1314.07	20547.21	151.08	722.08	−142.81
16	23909.64	1321.25	1313.99	20547.17	151.04	721.45	−145.26

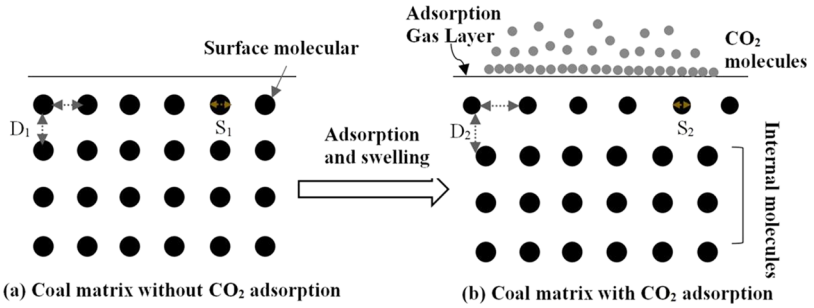

Figure 13. Conceptual diagram of sorptive matrix shrinkage and the swelling mechanism with intermolecular and surface forces. Reprinted (adapted or reprinted in part) with permission from AAPG Bulletin [Compressibility of sorptive porous media: Part 1. Background and theory]. Copyright [2014] [Shimin Liu;Satya Harpalani].

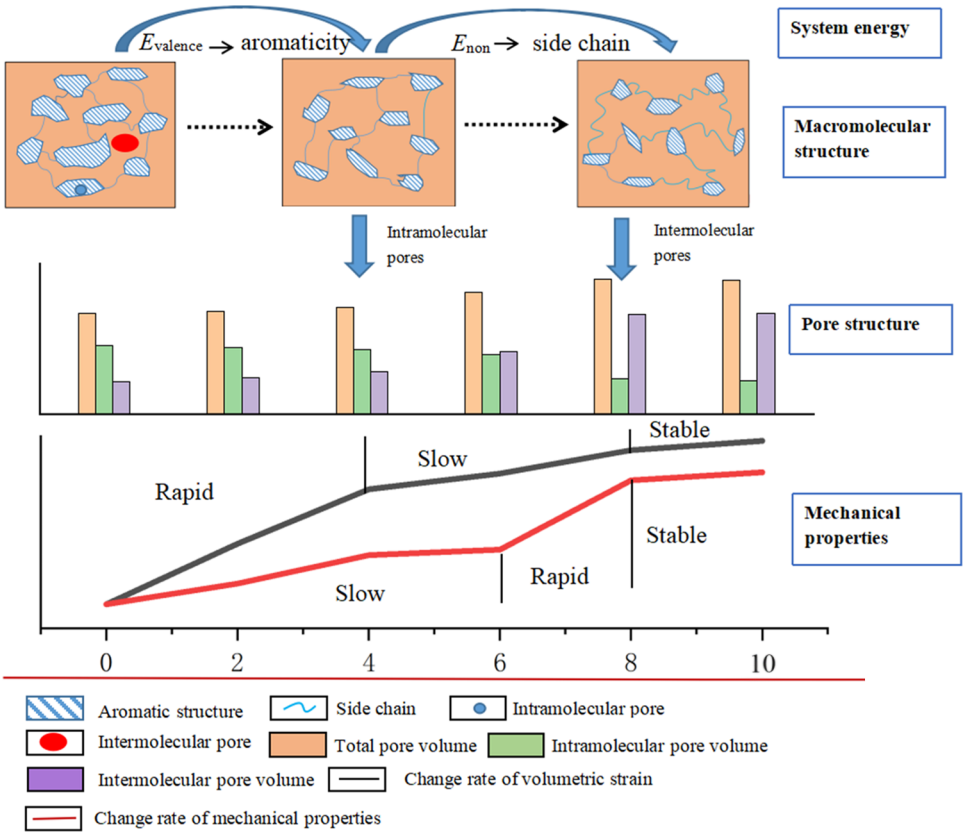

Figure 14. Relationship between pore structure, swelling strain, mechanical properties, chemical structure, and surface free energy.

3.5.2. Variation of E_{non} of Coal under Different CO_2 Injection Pressures. E_{non} is composed of van der Waals (E_{vdW}) energy and electrostatic energy (E_e), which represents the interaction between paired electrons. E_e is greater when the molecule has multiple charges or multipole moments. Coal molecules have high aromatic content and a large number of

https://doi.org/10.1021/acsomega.1c06566
ACS Omega 2022, 7, 6911−6923

aromatic rings, which leads to the $\pi-\pi$ stacking interaction in the molecular arrangement and controlled multipole moments of coal molecules. From Table 3, E_e changes from −127.3 to −145.26, which means that the multipole of coal molecules decreases, indicating that the aromatic structure is destroyed.

E_{vdW} is to stabilize the molecular system. E_{vdW} alternations include the following three situations: ① For molecules with a similar composition and structure, the greater the relative molecular mass, the greater the E_{vdW}, ② for a similar molecular structure, the higher the number of molecular side chains and the greater the distance between molecules, the smaller the E_{vdW}, and ③ uneven charge distribution of molecules reduces E_{vdW}. It can be seen from Table 3 that there is E_{vdW} reduction during the interaction between carbon dioxide and coal, indicating that the length of the aliphatic chain increases, the space obstruction effect becomes stronger, and the disorder degree of the molecular arrangement increases.

3.6. Mechanism of CZ Coal Swelling. Surface free energy is the potential energy of the molecules or atoms on the surface. Coal adsorbs CO_2 and induces swelling of the coal matrix, reducing coal surface free energy and leading to instability of the system. The molecules/atoms in the coal matrix tend to repel other molecules/atoms to achieve balance, leading to a rearrangement of the macromolecules in coal and changing the distance between the surface molecules and adjacent molecules, as shown in Figure 13.[61] The coal pore structure is related to the macromolecular structure. In high-rank coal, the intramolecular pores are associated with the interlayer spacing of the aromatic layers, and intermolecular pore volumes are determined by the directional arrangement of aromatic crystallites and the length of aliphatic hydrocarbon. The mechanical properties are not only related to the macromolecular structure but also related to the pore pressure; aliphatic chains lengthen, the aromaticity decreases, or the pore pressure increases, ultimately reducing the strength of coal. The relationship between pore structure, swelling strain, mechanical properties, chemical structure, and surface free energy is shown in Figure 14.

When pressure is at 0−4 MPa, the coal matrix adsorbs a large amount of CO_2, which causes the coal matrix to swell rapidly. $E_{valence}$ decreased from 23 451 to 23 333 Kcal/mol, and this shows that the content of the aromatic structure is reduced, leading to the intramolecular pore volume changing from 0.0340 to 0.0219 cm^3/g (corresponding to S1 changing to S2 in Figure 14). E_{vwD} decreased from 873.45 to 851.16 Kcal/mol, the distance between surface molecules and the adjacent molecules changes from D_1 to D_2 ($D_2 > D_1$), leading to the intermolecular pore volume changing from 0.0161 to 0.0211 cm^3/g. The decrease of aromatic structure and the increase of gas pressure are also accompanied by the weakening of mechanical properties.

When the pressure was at 4−8 MPa, the CO_2 pressure in pores increased, but the CO_2 adsorption amount increased slowly, and the coal matrix swelling induced by CO_2 adsorption can be resisted by external pressure. The higher pressure helps to form aliphatic hydrocarbons and increases the length of side chains and exacerbates system instability leading to the obvious decrease of E_{vdW} (from 851.16 to 768.24 Kcal/mol). The attraction force of CO_2 and coal molecules increased (the D_2 increases), resulting in the intermolecular pore increase (from 0.0211 to 0.0495 cm^3/g). H_{al}/H and CH_2/CH_3 increased, A_{ar}/A_{al} decreased, and pore pressure increased; especially when pressure is at 6−8 MPa, carbon dioxide is converted into a supercritical state, and the mechanical properties of coal change greatly.

Above 8 MPa, the pressure causes the internal structure to become very regular and compact. Hence, the volumetric swelling stops, and the pore structure and mechanical properties remain stable.

4. CONCLUSIONS

In this work, the various characteristics of pore structure, swelling strain, mechanical properties, chemical structure, and surface free energy were evaluated, and the mechanism of the CO_2−coal interaction in high-rank coal by molecular simulation was established. The conclusions of this study are as follows.

(1) By a comparative study of the experimental and simulation data, molecular simulation is found to be an effective method to study the coal matrix alterations during CO_2 injection into coal. The raw coal sample is more flexible than the coal macromolecular structure.

(2) CO_2 adsorption causes a significantly greater coal parameter alteration in high-rank coal. With the simulated coal's porosity increasing from 5.12 to 6.63%, UCS strength is reduced by up to around 54.59% with gas CO_2 adsorption and Young's modulus and Poisson's ratio are reduced and increased by around 70.43 and 73.07%, respectively. Furthermore, $ScCO_2$ with a higher adsorption capacity results in greater damage and causes larger alterations of coal parameters.

(3) The coal-swelling properties are controlled by molecular structure and surface free energy. $E_{valence}$ is a dominant factor in controlling the intramolecular and volumetric swelling strain. With decreasing $E_{valence}$, the aromaticity and size of the aromatic structure decrease, affecting the intramolecular pores and volumetric swelling strain. E_{non} maintains the stability of coal structure and mechanical properties, and the decrease of E_{non} indicates that the distance between the surface molecules becomes larger, leading to intermolecular pores increasing and mechanical properties weakening.

■ ASSOCIATED CONTENT

Supporting Information

The Supporting Information is available free of charge at https://pubs.acs.org/doi/10.1021/acsomega.1c06566.

CO_2 saturation-induced UCS; E and v alteration in CZ coal; and the relationship of pore structure, E, and v (PDF)

■ AUTHOR INFORMATION

Corresponding Author

Kui Dong − *Department of Geoscience and Engineering, Key Laboratory of Coal and Coal-measure Gas Geology in Shanxi Province, Taiyuan University of Technology, Taiyuan 030024, China;* orcid.org/0000-0003-2235-7089; Email: Dongkui1011@163.com

Authors

Zhiwei Zhai − *Shanxi Institute of Energy, Taiyuan 030006, China*

Bingyi Jia − *Xi'an Research Institute, China Coal Technology and Engineering Group Corp, Xi'an 710077, China*

Complete contact information is available at:

https://doi.org/10.1021/acsomega.1c06566
ACS Omega 2022, 7, 6911−6923

https://pubs.acs.org/10.1021/acsomega.1c06566

Author Contributions

All authors contributed equally to this work.

Notes

The authors declare no competing financial interest.

■ ACKNOWLEDGMENTS

K.D. and B.J. received funding from the National Natural Science Foundation of China (42103047) and the Applied Basic Research Project of Shanxi Province (20210302124644). Zhaizhi Wei received funding from the Shanxi Jinzhong Science and Technology Key Research and Development Plan (Y201026).

■ REFERENCES

(1) Fan, S.; Zhang, D.; Wen, H.; Cheng, X.; Liu, X.; Yu, Z.; Hu, B. Enhancing coalbed methane recovery with liquid CO_2 fracturing in underground coal mine: From experiment to field application. *Fuel* **2021**, *290*, No. 119793.

(2) Zhang, X.; Ranjith, P. Experimental investigation of effects of CO_2 injection on enhanced methane recovery in coal seam reservoirs. *J. CO_2. Util.* **2019**, *33*, 394−404.

(3) Kang, J.; Wan, R.; Zhou, F.; Liu, Y.; Li, Z.; Yin, Y. Effects of supercritical CO_2 extraction on adsorption characteristics of methane on different types of coals. *Chem. Eng. J.* **2020**, *388*, No. 123449.

(4) Hamidreza, Y.; Hamidreza, S.; Mohammad, M. Decision tree-based modeling of CO2 equilibrium absorption in different aqueous solutions of absorbents. *Environ. Prog. Sustainable Energy* **2019**, *38*, S441−S448.

(5) Yarveicy, H.; Mohammad, M.; Ghiasi, A. Performance evaluation of the machine learning approaches in modeling of CO_2 equilibrium absorption in Piperazine aqueous solution. *J. Mol. Liq.* **2018**, *255*, 375−383.

(6) Qin, C.; Jiang, Y.; Zhou, J.; Song, X.; Liu, Z.; Li, D.; et al. Effect of supercritical CO_2 extraction on CO_2/CH_4 competitive adsorption in Yanchang shale. *Chem. Eng. J.* **2021**, *412*, No. 128701.

(7) Lu, Y.; Liu, J.; Tang, J.; Ao, X.; Li, H.; et al. Pore changes of slickwater-containing shale under supercritical CO2 treatment. *Fuel* **2022**, *312*, No. 122775.

(8) Hosking, L.; Thomas, H. Dual porosity modelling of coal core flooding experiments with carbon dioxide. *Comput.Geotech.* **2020**, *121*, No. 103454.

(9) Niu, Q.; Cao, L.; Sang, S.; Wang, W.; Zhou, X.; et al. Experimental study on the softening effect and mechanism of anthracite with CO_2 injection. *Int. J. Rock. Mech. Min. Sci.* **2021**, *138*, No. 104614.

(10) Zofia, M.; Stanisław, M.; Jerzy, Z. Swelling and acoustic emission behaviour of unconfined and confined coal during sorption of CO_2. *Int. J. Coal. Geol.* **2013**, *116*, 17−25.

(11) Guo, H.; Wang, K.; Wu, Y.; Tang, H.; et al. Evaluation of the weakening behavior of gas on the coal strength and its quantitative influence on the coal deformation. *Int. J. Min. Sci. Techno.* **2021**, *31*, 451−462.

(12) Zagorščak, R.; Hywel, R. Effects of subcritical and supercritical CO_2 sorption on deformation and failure of high-rank coals. *Int. J. Coal. Geol.* **2018**, *199*, 113−123.

(13) Wang, S.; Derek, E.; Liu, J. Permeability evolution during progressive deformation of intact coal and implications for instability in underground coal seams. *Int. J. Rock. Mech. Min. Sci.* **2013**, *58*, 34−45.

(14) Zhao, L.; Guanhua, N.; Wen, Y.; Jiang, H.; et al. Analysis of permeability evolution mechanism during CO_2 enhanced coalbed methane recovery based on impact factor method. *Fuel* **2021**, *304*, No. 121389.

(15) Kang, J.; Ru, W.; Zhou, F.; Liu, Y.; Li, Z.; Yin, Y. Effects of supercritical CO_2 extraction on adsorption characteristics of methane on different types of coals. *Chem. Eng. J.* **2019**, *11*, No. 123449.

(16) Liu, S.; Sang, S.; Ma, J.; Wang, T.; Du, Y.; Fang, H. Effects of supercritical CO_2 on micropores in bituminous and anthracite coal. *Fuel* **2019**, *242*, 96−108.

(17) Zhang, K.; Cheng, Y.; Jin, K.; Guo, H.; Liu, Q.; et al. Effects of supercritical CO_2 fluids on pore morphology of coal: implications for CO_2 geological sequestration. *Energy Fuels* **2017**, *31*, 4731−4741.

(18) Liu, S.; Ma, J.; Sang, S.; Wang, T.; Du, Y.; Fang, H. The effects of supercritical CO_2 on mesopore and macropore structure in bituminous and anthracite coal. *Fuel* **2018**, *223*, 32−43.

(19) Ranjith, P.; Perera, M. Effects of cleat performance on strength reduction of coal in CO_2 sequestration. *Energy* **2012**, *45*, 1069−1075.

(20) Perera, M.; Ranjith, P.; Viete, D. Effects of gaseous and super-critical carbon dioxide saturation on the mechanical properties of bituminous coal from the Southern Sydney Basin. *Appl. Energy* **2013**, *110*, 73−81.

(21) Ranathunga, A.; Perera, M.; Ranjith, P.; Bui, H. Super-critical CO_2 saturation-induced mechanical property alterations in low rank coal: An experimental study. *J. Supercrit. Fluid.* **2016**, *109*, 134−140.

(22) Day, S.; Greg, D.; Richard, S.; Steve, Weir. Effect of coal properties on CO_2 sorption capacity under supercritical conditions. *Int. J. Greenh. Gas. Con.* **2008**, *2*, 342−352.

(23) Saghafi, A.; Faiz, M.; Robert, D. CO_2 storage and gas diffusivity properties of coals from Sydney Basin, Australia. *Int. J. Coal. Geol.* **2007**, *70*, 240−254.

(24) Griffith, A. A. The Phenomena of Rupture and Flow in Solids. *Philos. Trans. R. Soc., A* **1921**, *221*, 163−198.

(25) Larsen, J. The effects of dissolved CO_2 on coal structure and properties. *Int. J. Coal. Geol.* **2004**, *57*, 63−70.

(26) Zhang, B.; Zeng, F.; Wang, D.; Kang, G.; Zhang, X.; Kang, T. Macromolecular structure model of anthracite in southern Qinshui Basin and its methane bearing mechanical properties. *J. China. Coal. Soc.* **2021**, *46*, 534−543.

(27) Wang, K.; Pan, J.; Wang, E.; Hou, Q.; Yang, Y.; Wang, X. Potential impact of CO_2 injection into coal matrix in molecular terms. *Chem. Eng. J.* **2020**, *401*, No. 126071.

(28) Zhang, H.; Diao, R.; Hing, H.; Masood, M.; Brian, E. Molecular simulation of the adsorption-induced deformation during CO_2 sequestration in shale and coal carbon slit pores. *Fuel* **2020**, *272*, No. 117693.

(29) Xiang, J.; Zeng, F.; Li, B.; Zhang, L.; Li, M.; Liang, H. Construction of macromolecular structural model of anthracite from Chengzhuang coal mine and its molecular simulation. *J. Fuel Chem. Techno.* **2013**, *41*, 391−400.

(30) Liu, Y.; Zhu, Y.; Li, Wu.; Xiang, J.; Wang, Y.; Li, J.; Zeng, F. Molecular simulation of methane adsorption in shale based on grand canonical Monte Carlo method and pore size distribution. *J. Nat. Gas. Sci. Eng.* **2016**, *30*, 119−126.

(31) Lu, H.; Li, X.; Zhang, C.; Chen, J.; Ma, L.; Li, W.; Xu, D. Experiments and molecular dynamics simulations on the adsorption of naphthalene sulfonic formaldehyde condensates at the coal-water interface. *Fuel* **2020**, *264*, No. 116838.

(32) Song, Y.; Jiang, B.; Lan, F. Competitive adsorption of $CO_2/N_2/CH_4$ onto coal vitrinite macromolecular: Effects of electrostatic interactions and oxygen functionalities. *Fuel* **2019**, *01*, 23−28.

(33) Asem, P. Prediction of unconfined compressive strength and deformation modulus of weak argillaceous rocks based on the standard penetration test. *Int. J. Rock. Mech. Min.* **2020**, *133*, No. 104397.

(34) Li, L.; Zhang, X.; Wang, Y. Influence of pre-electrical stress on microstructure and breakdown property of polymer. *H. Vol. Eng.* **2017**, *43*, 2866−2874.

(35) Hossain, D.; Tschopp, M.; Ward, D.; Bouvard, J.; Wang, P.; et al. Molecular dynamics simulations of deformation mechanisms of amorphous polyethylene. *Polymer* **2010**, *51*, 6071−6083.

(36) Kimura, K.; Yajima, M.; Tominaga, Y. A highly-concentrated poly(ethylene carbonate)-based electrolyte for all-solid-state Li battery working at room temperature. *Electrochem. Commun.* **2016**, *66*, 46−48.

(37) Lin, J.; Ren, T.; Cheng, Y.; Nemcik, J.; Wang, G. Cyclic N_2 injection for enhanced coal seam gas recovery: a laboratory study. *Energy* **2019**, *188*, No. 116115.

(38) Liu, S.; Harpalani, S. A new theoretical approach to model sorption-induced coal shrinkage or swelling. *AAPG Bull.* **2013**, *97*, 1033−1049.
(39) Scherer, G. Dilation of porous glass. *J. Am. Ceram. Soc.* **1986**, *69*, 473−480.
(40) Goodman, R. *Introduction to Rock Mechanics*; John Wiley Sons: New York, 1980; 173pp.
(41) Zhao, W.; Wang, K.; Liu, S.; Ju, Y.; Zhou, H.; Fan, L.; Yang, Y.; Cheng, Y.; Zhang, X. Asynchronous difference in dynamic characteristics of adsorption swelling and mechanical compression of coal: Modeling and experiments. *Int. J. Rock. Mech. Min.* **2020**, *135*, No. 104498.
(42) Pan, Z.; Luke, D. A theoretical model for gas adsorption-induced coal swelling. *Int. J. Coal. Geol.* **2007**, *69*, 243−252.
(43) Wang, R.; Wang, Q.; Niu, Q.; Pan, J.; Wang, H.; Wang, Z. CO_2 adsorption and swelling of coal under constrained conditions and their stage-change relationship. *J. Nat. Gas. Sci. Eng.* **2020**, *76*, No. 103205.
(44) Liu, Y.; Zhu, Y.; Li, W.; Zhang, C.; Wang, Y. Ultra micropores in macromolecular structure of subbituminous coal vitrinite. *Fuel* **2017**, *210*, 298−306.
(45) Sarkisov, L.; Harrison, A. Computational structure characterisation tools in application to ordered and disordered porous materials. *Mol. Simulat.* **2011**, *37*, 1248−1257.
(46) Chen, K.; Liu, X.; Wang, L.; Song, D.; Nie, B.; Yang, Tao. Influence of sequestered supercritical CO2 treatment on the pore size distribution of coal across the rank range. *Fuel* **2021**, *306*, No. 121708.
(47) Gao, S.; Jia, L.; Zhou, Q.; Cheng, H.; Wang, Y. Microscopic pore structure changes in coal induced by a CO2-H2O reaction system. *J. Pet. Sci. Eng.* **2022**, *208*, No. 109361.
(48) Cheng, Y.; Zhang, X.; Lu, Z.; Pan, Z.; Zeng, M.; et al. The effect of subcritical and supercritical CO_2 on the pore structure of bituminous coals. *J. Nat. Gas. Sci. Eng.* **2021**, *94*, No. 104132.
(49) Maya, J. C.; Macías, C.; Gómez, F.; et al. On the evolution of pore microstructure during coal char activation with steam/CO_2 mixtures. *Carbon* **2020**, *158*, 121−130.
(50) Liu, C.; Wang, G.; Sang, S.; Gilani, W.; Rudolph, V. Fractal analysis in pore structure of coal under conditions of CO_2 sequestration process. *Fuel* **2015**, *139*, 125−132.
(51) GB/T 21650.1-2008. *Pore Size Distribution and Porosity of Solid Materials by Mercury Porosimetry and Gas Adsorption-Part 1: Mercury Porosimetry*; China Quality and Standards Publishing & Media Co., Ltd.: Beijing, 2008.
(52) GB/T 21650.3-2011. *Pore Size Distribution and Porosity of Solid Materials by Mercury Porosimetry and Gas Adsorption-Part 3: Analysis of Micropores by Gas Adsorption*; China Quality and Standards Publishing & Media Co., Ltd.: Beijing, 2011.
(53) Song, D.; Ji, X.; Li, Y.; Zhao, H.; Song, B.; He, K. Heterogeneous development of micropores in medium-high rank coal and its relationship with adsorption capacity. *Int. J. Coal. Geol.* **2020**, *226*, No. 103497.
(54) Zeng, Q.; Wang, Z.; Liu, L.; Ye, J.; McPherson, B.; McLennan, J. Modeling CH_4 displacement by CO_2 in deformed coalbeds during enhanced coalbed methane recovery. *Energy Fuels* **2018**, *32*, 1942−55.
(55) Masoudian, M.; Airey, D.; Zein, A. Experimental investigations on the effect of CO_2 on mechanics of coal. *Int. J. Coal. Geol.* **2014**, *128*−*129*, 12−23.
(56) Li, M.; Pang, B.; Su, E.; Liu, Q.; Cheng, Y. Time-dependence of mechanical property alterations on anthracite coals treated by supercritical carbon dioxide. *Geofluids* **2019**, *2019*, 1−9.
(57) Long, H.; Lin, H.; Yan, M.; Chang, P.; Li, S.; Bai, Y. Molecular simulation of the competitive adsorption characteristics of CH_4, CO_2, N_2, and multicomponent gases in coal. *Powder Technol.* **2021**, *385*, 348−356.
(58) Meng, Y.; Li, Z. Experimental comparisons of gas adsorption, sorption induced strain, diffusivity and permeability for low and high rank coals. *Fuel* **2018**, *234*, 914−923.
(59) Dong, K.; Zhai, Z.; Guo, A. Effects of pore parameters and functional groups in coal on CO_2/CH_4 adsorption. *ACS Omega* **2021**, *6*, 32395−32407.
(60) Lin, S.; Liu, Z.; Zhao, E.; Qian, J.; Li, X.; et al. A study on the FTIR spectra of pre- and post-explosion coal dust to evaluate the effect of functional groups on dust explosion. *Process. Saf. Environ.* **2019**, *130*, 48−56.
(61) Liu, S.; Harpalani, S. Compressibility of sorptive porous media: Part 1.Background and theory. *AAPG Bull.* **2014**, *98*, 1761−1772.

https://doi.org/10.1021/acsomega.1c06566
ACS Omega 2022, 7, 6911−6923